We thank the two anonymous reviewers and the editor for your extensive general and specific comments that addressed important issues which help us to improve the quality of the manuscript significantly.

Anonymous Referee #1

Although one of the major issues of the first round of reviews (style and language) has improved, I stopped reviewing the manuscript after reading the Abstract and the Introduction. There are still too many issues that need correction, even if most of them could be considered as minor, like the usage of not introduced abbreviations in the Abstract, wrong format of citations, spelling of the term "River" etc. and a few grammatically incorrect sentences. This is really a pity, because content-wise the manuscript has a good potential to be published, but such issues should not occur in a manuscript submitted after the first revisions.

Anonymous Referee #2

The paper improved substantially and the comments have been addressed adequately, though some questions remain (see comments in file attached). However, the spelling and grammar is still inadequate. We stopped correcting the mistakes after the first sections, because it was to tedious.

This was already commented by both previous reviewers. The authors responded: "accepted and the authors tried at their best to improve the quality of the language significantly." This is, however, not enough for a scientific paper. Please let a native speaker review the paper before the next submission.

Response from the authors:

All comments from both referees and from the editor which focused on the language, spelling and grammar usage are accepted. We have tried to improve the language substantially and corrected the spelling errors and grammatically incorrect sentences to our best. Here, we would like to mention that the manuscript has been proofread by the native speaker as well. The corrections and improvements made for the specific and general comments from the two anonymous referees have shown in the markedup manuscript as below.

# Analysis of the combined and isolated~~single~~ effects of LULC and climate change on ~~the streamflow of~~ the Upper Blue Nile River Basin's streamflow u~~U~~sing statistical trend tests, remote sensing land-cover maps, and the SWAT model

Dagnenet F. Mekonnen[1, 2], Zheng Duan[1], Tom Rientjes[3], Markus Disse[1]

[1]Chair of Hydrology and River Basin Management, Faculty of Civil, Geo and Environmental Engineering, Technische Universität München, Arcisstrasse 21, 80333, Munich, Germany.
[2]Amhara Regional State Water, Irrigation and Energy Development Bureau, Bahirdar, Ethiopia
[3]Department of Water Resources, Faculty of Geo-Information Science and Earth Observation (ITC), University of Twente, Enschede, Netherlands
Correspondence to: Dagnenet F. (dagnfenta@yahoo.com)

**Abstract:** Understanding the response of land use/land cover (LULC) change and climate change to the streamflow of the Nile River has ~~become~~ a priority issue for water management and water resource utilization in~~of~~ the Nile basin. This study assesses the long-term trends of rainfall and streamflow to ~~analyse~~ analyze the ~~response~~ effect of LULC and climate changes on the hydrology of the ~~study area~~ Upper Blue Nile River basin. The Mann-Kendal (MK~~)~~) test showed ~~—~~ statistically insignificant, increasing trends for annual, monthly, and long rainy-season rainfall series wh~~ereas~~ile no trend for daily, short rainy, and dry season rainfall series ~~appeared~~. However, the Pettitt test failed to~~could not~~ detect any jump point in basin-wide rainfall series except for daily rainfall time series. In contrast, the ~~result of the~~ MK test's result for daily, monthly, annual, and seasonal (long and short rainy season and dry season) time-series streamflow showed a statistically significant, positive trend ~~and the trend magnitude is statistically significant~~. Landsat satellite images for 1973, 1985, 1995, and 2010 were used for LULC change detection analysis. The LULC change detection findings indicate significant~~that~~ expansion of cultivated land area and the reduction of forest coverage ~~were significant~~ before ~~the period~~ 1995 ~~period~~. After 1995, the forest coverage ~~began to~~ increased while the amount of cultivated land diminish~~ getting reduc~~ed. Statistically, forest coverage changed from 17.4 % to 14.4 %, 12.2 %, and 15.6 % while cultivated land changed from 62.9 % ~~—~~ to 65.6 %, 67.5 %, and 63.9 % ~~—~~ from 1973 to 1985, in 1995, and in 2010 respectively. The hydrological ~~—~~ model result showed that mean annual streamflow increased by 16.9 % between the 1970s and the 2000s due to the combined effect of LULC and climate change. The ~~single~~isolated effect of LULC change on streamflow ~~analysis~~ suggested that LULC change affects surface ~~run-off~~runoff and base flow. This could be attributed to the 5.1 % reduction in forest coverage and 4.6 % increase in cultivated land area. Effects of climate change revealed that the increased rainfall intensity and number of extreme rainfall events from 1971 to 2010 have significantly affected the surface ~~run off~~runoff and base flow. The ~~single~~isolated impacts of climate change are ~~is~~ more significant as compared to the impacts of LULC change for the hydrology of ~~UBNRB~~ the study area.

# 1. Introduction

The Abay (Upper Blue Nile) River in Ethiopia contributes more than 60 % of the water resources of the Nile River (McCartney et al., 2012). Hence, the Ethiopian government has conducted a series of studies to tap this huge potential water resource with intent to significantly increase the number of large water-storage reservoirs in the Upper Blue Nile River Basin (UBNRB), both for irrigation and hydropower development, to support national development and reduce poverty (BCEOM, 1998). As a result, large-scale irrigation and hydropower projects such as the Grand Ethiopian Renaissance Dam (GERD), which will be the largest dam in Africa after it is completed, have been planned and realized along the main stem of the Blue Nile River. However, its hydrology exhibiting high seasonal flows, is influenced by large variations in climate, altitude/topography, and land use/cover (LULC) change. Therefore, effective planning, management, and regulation of water resource developments is therefore required to avert conflicts between the competing water users particularly with the downstream countries of Sudan and Egypt. Establishing careful water resource management can mitigate potential conflicts and maximize benefits.

Only understanding the hydrological processes and sources impacting water quantity, such as LULC change and climate change, can achieve this as they are the key driving forces that can modify the watershed's hydrology and water availability (Oki and Kanae, 2006; Woldesenbet *et al.*, 2017b; Yin *et al.*, 2017a). LULC change can modify the rainfall path into runoff by altering critical water balance components, such as surface runoff, groundwater recharge, infiltration, interception, and evaporation (Marhaento et al., 2017; Woldesenbet et al., 2017b). The UBNRB experiences significant spatial and temporal climate variability (McCartney et al. 2012). Less than 500 mm of precipitation falls annually near the Sudanese border whereas more than 2,000 mm falls annually in some places of the southern basin (Awulachew et al., 2009). Potential evapotranspiration (ET) also varies considerably and is strongly correlated with altitude. It varies from more than 2,200 mm annually near the Sudanese border from between about 1,300 mm and 1,700 mm annually in the Ethiopian highlands (McCartney et al., 2012). The precipitation and ET cycles cause extreme seasonal and inter-annual variability, to strongly characterize stream flow.

A literature review shows that few sub-basin and basin-level studies are conducted in the UBNRB. Most of the studies were focused on trend analysis of precipitation and streamflow. For example those by (Bewket and Sterk, 2005; Cheung *et al.*, 2008; Conway, 2000; Gebremicael *et al.*, 2013; Melesse *et al.*, 2009; Rientjes *et al.*, 2011; Seleshi and Zanke, 2004; Teferi *et al.*, 2013; Tekleab *et al.*, 2014; Tesemma *et al.*, 2010). reported no significant trend in annual and seasonal precipitation totals within the Lake Tana sub-

basin, wWhereasile Mengistu et al. (2014) reported statistically non -significant increasing trends inat annual and seasonal rainfall series, except for a short rainy season (Belg-) from February to May.

For the streamflow of the UBNRB, Gebremicael *et al.* (2013) reported statistically significant increasing long-term mean annual streamflow at the El Diem gauging station for the UBNRB's streamflow. However, (Tesemma *et al.*, 2010) reported no statistically significant trend for the long- term annual streamflow at the ElDiem gauging station, but did report a significantly increasing trend at the Bahirdar and Kessie stations. At the sub-basinsub-basin scale, Rientjes et al. (2011) reported a decreasing trend for the low streamflows of Gilgel Abay sub-basinsub-basin (Lake Tana catchment, the Blue Nile headwaters) during the period (1973–2005 period), specifically by 18.1 % and 66.6 % in the periods 1982–2000 and 2001–2005, respectively. However, for the same periods, the high streamflows for the same periods show an increase by 7.6 % and 46.6 % due to LULC change and seasonal rainfall variability of rainfall.

Although, substantial progress has been made in assessing the impacts of LULC and climate changes on the UBNRB's hydrology of the UBNRB, only a few studies have endeavorattempted to assess the attribution of changes in the water balance to LULC change and climate change. Woldesenbet et al. (2017b), used an integrated approach comprising SWAT hydrological modeling and partial least squares regression (PLSR) to quantify the contributions of changes in individual LULC classes to changes in hydrological components in thewo watersheds namely: Lake Tana and Beles sub-basinsubbasins' watersheds. Woldesenbet *et al.* (2017b) reported that expansion of cultivation land area and decline in woody shrub/woodland appear to be major environmental stressors affecting local water resources such as increasing surface run offrunoff and decreasing of ground water contribution in both watersheds; however,but the impacts of climate change is missing were not considered. NonethelessHowever, proper water –resource management requires an in-depth understanding ofn the aggregated and disaggregated effects of LULC and climate changes on streamflow and water balance components as the interaction between LULC, the climate characteristics, and the underlying hydrological processes are complex and dynaanmic (Yin *et al.*, 2017a). .

Therefore, the objectives of this study's objectives are as followstherefore to (i) assess the long-term trend of rainfall and streamflow (ii) analyzzse the LULC change, and (iii) examining the streamflow responses to the combined and isolated effects of LULC and climate changes in the UBNRB. This iscan be doablene byusing a combininged analysis of statistical trend test, change detection of LULC derived from satellite remote sensing, and hydrological modelling during the period 1971–2010 period.

## 2. Study area

The UBNRB is located in northwestern Ethiopia. Its catchment area is about 172,760 km². Highlands, hills, valleys, and occasional rock peaks with elevations ranging from 500 m.a.s.l to above 4000 m.a.s.l typically characterize the basin's topography (Figure 1). According to BCEOM (1998), two thirds of the basin lies in Ethiopia's highlands with annual rainfall ranging from 800 mm to 2,200 mm. A central and south-eastern area is characterized by relatively high rainfall (1400 mm to 2200 mm) although less than 1200 mm rain fell in most of the eastern and north-western parts of the basin. Mekonnen and Disse (2018) showed that the UBNRB has a mean areal annual rainfall of 1452 mm and mean annual minimum and maximum temperatures of 11.4 °C and 24.7 °C respectively.

Tropical climate characterizes the study area, which is dominated by its high altitude. Movement of the Inter-Tropical Convergent Zone (ITCZ) also governs the climate (Conway, 2000; Mohamed et al., 2005). NMA (2013) classified the climate into three seasons in Ethiopia. The main rainy season (Kiremt) generally lasts from June to September during which south-west winds bring rains from the Atlantic Ocean. Some 70–90 % of the total rainfall occurs during this season. A dry season (Bega) lasts from October to January and the short rainy season (Belg) lasts from February to May. According to BCEOM (1998), the average annual discharge is estimated about 49.4 Billion Cubic Meter (BCM), with the low-flow month (April) equivalent to less than 2.5 % of that of the high-flow month (August), at the Ethio-Sudan border (El Diem). The analysis of this study revealed that the long-term (1971–2010) mean annual volume of flow at El Diem is 50.7 BCM, with the low flow (dry season) contributing 21.1 % and the short rainy season accounting for about 6.2 %. Whereas most flow occurred during the rainy season, contributing about 73 % (Table 1). The basin's land cover essentially follows the divide between highland and lowland. Predominantly farmlands (about 90 %), bush, and shrubs cover the highlands. The lowlands, in contrast, are still largely untouched by development. As a result, woodlands, bush, and shrub lands are the dominant forms of land cover (BCEOM, 1998).

## 3. Input data sources

In this study, non-parametric Mann-Kendal (MK) (Kendall, 1975; Mann, 1945) statistics and the Soil and Water Assessment Tool (SWAT), developed by the Agricultural Research Service of the United States Department of Agriculture (USDA-ARS) (Arnold et al., 1998), are used for statistical trend analysis and water-balance modelling respectively. The methods' details are described under section 4. The input datasets used for the SWAT model can be categorized into those containing weather and streamflow data, and spatially distributed datasets.

### 3.1 Weather and streamflow data

The daily weather variables used in this study for trend analysis and for driving the water-balance model are precipitation, minimum air temperature (Tmin), maximum air temperature (Tmax), relative humidity (RH), hours of sunshine (SH), and wind speed (WS). These weather data were obtained from the Ethiopian National Meteorological Service Agency (ENMSA) for the 1971–2010 period. The daily streamflow data for over 25 gauging stations was collected from the Federal Ministry of Water, Irrigation and Electricity of Ethiopia for the 1971–2010 period. After intensive and rigorous analyses of the weather data, a considerable amount of time-series data were found to be missed in most of the stations (see Table S01). The occurrences of civil war, defective and outdated devices were the main causes for the missing data records. As a result, the available data constrained us to focus on only 15 stations (Figure 1) in which rainfall data is relatively more complete. All 15 stations were used for trend analysis whereas the 10 stations having complete climate variables, such as Tmax, Tmin, RH, WS, and SH were used as input for the SWAT model Figure 1.

We used spatial interpolation techniques, such as the inverse distance weighting method (IDWM), and linear regression techniques (LR) to fill the gaps. Uhlenbrook et al. (2010) applied similar approaches or methods for the Gilgel Abbay sub-basin, which is the UBNRB's headwater. The selection and number of adjacent stations are critically important for the accuracy of the estimated results. As mentioned by Woldesenbet et al. (2017a), different authors used different criteria to select neighboring stations. Because of study area's low station density, a geographic distance of 100 km were considered for most stations when selecting neighbouring stations. If no station is located within 100 km of the target station, then the search distance is increased until at least one suitable station is reached. After the neighbouring stations were selected, the two methods (IDWM and LR) were tested to fill in missing datasets. The candidate methods' performances were evaluated using the statistical metrics such as root mean square error (RMSE), mean absolute error (MAE), correlation coefficient ($R^2$), and percent bias (% bias) between observed and estimated values for the target stations. Equally weighted statistical metrics are applied to compare the performances of selected methods at target stations and establish ranking. A score was assigned to each candidate method according to the individual metrics. For example, the candidate achieving the smallest RMSE and MAE, or % bias got score 1, and so on. The final score is obtained by summing up the score pertaining to each candidate approaches at each station. The method with smallest score is the best. The monthly, seasonal, and annual weather data were aggregated from the daily time-series data after filling the gaps. While filling in the missing data, uncertainty is expected due to low station density, poor correlations, and the considerable number of missing records. Similar techniques and approaches were used for the analysis and filling in of missing streamflow data records.

**3.2 Spatial Data**

Required spatially distributed data required for the SWAT model includes tabular and spatial soil data, tabular and spatial land use /cover information, and elevation data. A Shuttle Radar Topographic Mission Digital Elevation Model (SRTM DEM) of 90 meters' resolution from the Consultative Group on International Agricultural Research-Consortium for Spatial Information (CGIAR-CSI; http://srtm.csi.cgiar.org/SELECTION/inputCoord.asp) was used to delineate the watershed and to analyze the land surface terrain's drainage patterns. Sub-basin parameters such as slope gradient, slope length of the terrain, and the stream network characteristics such as channel slope, length, and width were derived from the DEM.

The soil map developed by the Food and Agriculture Organization of the United Nations (FAO-UNESCO) at a scale of 1:5,000,000 and downloaded from http://www.fao.org/soils-portal/soil-survey/soil-maps-and-databases/faounesco-soil-map-ofthe-world/en/ was used for the SWAT model. Soil information such as soil textural and physiochemical properties needed for the SWAT model was extracted from Harmonized World Soil Database v1.2, a database that combines existing regional and national soil information (http://www.fao.org/soils-portal/soil-survey/soil-maps-and-databases/harmonized-world-soil-databasev12/en/) with information provided by the FAO-UNESCO soil map (Polanco et al., 2017).

The LULC maps, representing one of the most important driving factors affecting surface runoff and evapo-transpiration in a basin were produced from satellite remote sensing Landsat images for 1973, 1985, 1995, and 2010 at a scale of 30 m x 30 m resolution. Detailed image processing and classification approaches are described under section 4.2.

**4. Methodology**

**4.1 Trend Analysis**

The non-parametric Mann-Kendal (MK) (Kendall, 1975; Mann, 1945) statistic is chosen to detect trends for precipitation and streamflow time series data as it is widely used for effective water resource planning, design, and management (Yue and Wang, 2004). Its advantage over parametric tests such as t-test is that the MK test is more suitable for non-normally distributed and missing data, which are frequently encountered in hydrological time series (Yue et al., 2004). However, the existence of positive serial correlation in time series data affects the MK test result. If serial correlation exists in time series data, the MK test rejects the null hypothesis of no trend detection more often than specified by the significance level (von Storch, 1995).

~~In order to limit the influence of serial correlation on the MK test, pre-whitening was proposed by~~ von Storch (1995) proposed prewhitening to limit the influence of serial correlation on the MK test. T~~And also, t~~he Effective or Equivalent Sample Size (ESS) method developed by Hamed and Rao (1998) has also been proposed to modify the variance. However, the study by (Yue *et al.*, 2002) reported that von Stroch's pre-whitening is effective only when no trend exists and the ~~rejection rate of the~~ ESS approach's rejection rate after modifying the variance is much higher than the actual (Yue et al., 2004). ~~Then,~~ Yue et al. (2002) then proposed trend-free pre-whitening (TFPW) prior to applying the MK trend test in order to minimize it's limitation. This study therefore employed TFPW to remove the serial correlation and to detect a trend in a time -data series with significant serial correlation. Further details can be found in (Yue et al., 2002). All the trend results in this paper have been evaluated at the 5 % level of significance to ensure ~~an~~ effective exploration of the trend characteristics within the study area.

**Change point test**

The Pettitt test is used to identify whether or not~~if~~ there is a point change or jump in the data series (Pettitt, 1979). This method detects one unknown change point by considering a sequence of random variables, X 1, X 2, …, XT~~,~~ that may have a change point at N if Xt for t = 1, 2, …, N has a common distribution function, F1(x) ~~,~~and ~~a nd~~ Xt for t = N + 1, …, T has a common distribution function, F2(x), and F1(x) ≠ F-2(x).

**Sen's slope estimator**

The trend magnitude is estimated using a non-parametric median--based slope estimator proposed by (Sen, 1968) as it is not greatly affected by gross data errors or outliers, and ~~it~~ can be computed when data is~~are~~ missing. The slope estimation is given by~~:~~

$$\beta = \text{Median} \left[ \frac{x_j - x_k}{j - k} \right] \text{ for all } k < j, \hspace{4cm} (1)$$

w~~W~~here 1 < k < j < n, and β is considered as the median of all possible combinations of pairs for the whole data set. A positive value of β indicates an upward (increasing) trend and a negative value indicates a downward (decreasing) trend in the time series. All MK trend tests, Pettitt change--point detections, and S~~s~~en's slope analyses were conducted using the XLSTAT add-ins tool from excel (www.xlstat.com).

**4.2 Remote sensing land use/cover map**

**4.2.1. Landsat image acquisition**

Landsat images from~~of~~ the years 1973, 1985, 1995, and 2010 were accessed free -of -charge from the US Geological Survey (USGS) Center for Earth Resources Observation and Science (EROS) via http://glovis.usgs.gov. The Landsat image scenes

were selected based on the criteria of acquisition period, availability, and percentage of cloud cover. (Hayes and Sader, 2001), recommend acquiring images from the same acquisition period to reduce scene-to-scene variation caused by sun angle, soil moisture, atmospheric condition, and vegetation phenology differences. Hence, cloud free images were hence collected for the dry months of January to May. However, as the basin covers a large area, each of the LULC map's periods comprised 16 Landsat scenes. Accessing all the scenes during a dry season in a single year was therefore difficult. Hence, images were acquired ±1 year for each time period and some images were also acquired in the months of November and December. For example, 16 Landsat MSS image scenes were acquired in 1973 (10 images in January, 4 images in December and 2 images in November (±1 years) and merged to arrive at one LULC representation for selected years. Please see supplement Table s02 for the details on Landsat images.

### 4.2.2 Pre-processing and processing images

Several standard pre-processing methods including geometric and radiometric correction were implemented to prepare the LULC maps from Landsat images. Although many different classification methods exist, supervised and unsupervised classifications are the two most widely used methods for landcover classification from remote-sensing images. Hence, in this study, a hybrid supervised/unsupervised classification approach was adopted to classify the images from 2010 (LandsatTM). Iterative Self-Organizing Data Analysis (ISODATA) clustering was first performed to determine the image's spectral classes or land cover classes. Polygons for all of the training samples based on the identified LULC classes were then digitized using ground truth data. The samples for each land cover type were then aggregated. Finally, a supervised classification was performed using a maximum likelihood algorithm to extract four LULC classes.

A total of 488 Ground Control Points (GCPs) regarding landcover types and their spatial locations were collected from field observation in March and April 2017 using a Global Positioning System (GPS). Reference data (GCPs) was collected and taken from areas where there had not been any significant landcover change between 2017 and 2010. These areas were identified by interviewing local elderly people, and supplemented using high resolution Google Earth Images and the first author's priori knowledge. As many as 288 points were used for accuracy assessment and 200 points were used for developing training sites to generate a signature for each land-cover type. The classifications' accuracy was assessed by computing the error matrix (also known as the confusion matrix), which compares the classification result with ground truth information as suggested by DeFries and Chan (2000). A confusion matrix lists the values for the reference data's known cover types in the columns and for the classified data in the rows (Banko, 1998) as shown in Table 5. From the confusion matrix, a statistical metrics of overall accuracy, producers' accuracy

and users' accuracy are used. Another discrete multivariate technique ~~of~~ use~~ful~~ in accuracy assessment is called KAPPA (Congalton, 1991). The statistical metric~~s~~ for KAPPA analysis is ~~the~~a Kappa coefficient, which is another measure of the proportion of agreement or accuracy. The Kappa coefficient is computed as

$$K = \frac{N \sum_{i=1}^{i=r} x_{ii} \sum_{i=1}^{r}(x_{i+} * x_{+i})}{N^2 - \sum_{i=1}^{r}(x_{i+} * x_{+i})} \tag{2}$$

where r is the number of rows in the matrix, $x_{ii}$ is the number of observations in row i and column i, $x_{i+}$ and $x_{+i}$ are the marginal totals of row i and column i, respectively.~~, and~~ N is the total number of observations.

Once the landcover classification of the year 2010 Landsat image had been~~is~~ completed and its accuracy ~~is~~ checked, the
10 NDVI differencing technique (Mancino *et al.*, 2014) was applied to classify the images from~~of~~ 1973, 1985, and 1995. This technique was chosen to increase the accuracy of classification as it is hard to find an accurately classified digital or analog~~ue~~ LULC map of the study area during ~~the period of~~ 1973, 1985, and 1995. T~~And also, t~~he information obtained from the elders is~~are~~ also more subjective and its reliability is questionable when there is considerable time gap. We first calculated the NDVI from the Landsat MSS (1973) and three pre-processed Landsat TM images (1985, 1995, and 2010)
15 following the general normalized difference between band TM4 and band TM3 images ~~(ee~~(eqn. 3). The resulting successive NDVI images were subtracted each other to assess the ΔNDVI image with positive (vegetation increase), negative (vegetation cleared) and no change at~~on~~ a 30-m x 30 m pixel resolution (eqs~~n~~.4–6). The Landsat MSS 60 m x 60 m pixel-size data sets were resampled to a 30 m x 30 m pixel size using the "nearest neighbo~~ur~~" technique ~~in order~~ to have similar pixel sizes for the different images without altering the image data's original pixel values ~~of the image data~~.

$$NDVI = \frac{(TM4 - TM3)}{(TM4 + TM3)} \text{ or } \frac{(MSS_3 - MSS_2)}{(MSS_3 + MSS_2)} \tag{3}$$

$$\Delta NDVI_{1995/2010} = NDVI_{1995} - NDVI_{2010} \tag{4}$$

$$\Delta NDVI_{1985/1995} = NDVI_{1985} - NDVI_{1995} \tag{5}$$

$$\Delta NDVI_{1973/1985} = NDVI_{1973} - NDVI_{1985} \tag{6}$$

25 The ΔNDVI image was then reclassified using a threshold value calculated as $\mu \pm n*\sigma$; where μ represents the ΔNDVI pixels value mean, and σ the standard deviation. The threshold identifies three ranges in the normal distribution: (a) the left tail ($\Delta NDVI < \mu - n*\sigma$),~~;~~ (b) the right tail ($\Delta NDVI > \mu + n*\sigma$),~~;~~ and (c) the central region of the normal distribution ($\mu - n*\sigma < \Delta NDVI < \mu + n*\sigma$). Pixels within the two tails of the distribution are characterized by significant landcover changes, ~~while~~ whereas pixels in the central region represent no change. To be more conservative, n = 1 was selected for this study to

narrow the ~~threshold~~ ranges ~~of the threshold~~ for reliable classification. The standard deviation (σ) is one of the most widely applied threshold identification approaches for different natural environments based on different remotely sensed imagery (Hu *et al.*, 2004; Jensen, 1996; Lu *et al.*, 2004; Mancino *et al.*, 2014; Singh, 1989) as cited by Mancino *et al.* (2014).

ΔNDVI pixel values (2010–1995) in the central region of the normal distribution (μ – n·σ < ΔNDVI < μ + n·σ) represent an absence of landcover change between two different periods (i.e., 1995 and 2010); therefore, pixels from~~of~~ 1995 corresponding to no landcover change can be classified as similar to the 2010 landcover classes. Pixels with significant NDVI change are again classified using supervised classification, taking signatures from the already classified, no-change pixels. Likewise, ~~landcover classification of~~ 1985 and 1973 landcover images were~~as~~ ~~performed~~ classified based on the classified images of 1995 and 1985 respectively. Finally, after classifying the raw ~~images of~~ Landsat images into different landcover classes, change detection, which requires the comparison of independently produced classified images (Singb, 1989), was performed by the post-classification method. The post-classification change-detection comparison was conducted to determine changes in LULC between two independently classified maps from images of two different dates. Although this technique has some limitations, it is the most common approach because~~as~~ it does not require data normalization between two dates (Singh, 1989). This is because data from two dates are separately classified, thereby minimizing the problem of normalizing for atmospheric and sensor differences between two dates.

## 4.3 SWAT hydrological model

The Soil and Water Assessment Tool (SWAT) is ~~an~~ an open-source-code, semi-distributed model with a large and growing number of model applications in a variety of studies ranging from catchment to continental scales (Allen *et al.*, 1998; Arnold *et al.*, 2012; Neitsch *et al.*, 2002). It enables ~~to evaluates~~ the impact of LULC change and climate change on water resources to be evaluated in a basin with varying soil, land use, and management practices over a set period of time (Arnold *et al.*, 2012).

In SWAT, the watershed is divided into multiple sub-basins, which are further subdivided into hydrological response units (HRUs) consisting of homogeneous land-use management, slope, and soil characteristics (Arnold *et al.*, 2012; Arnold *et al.*, 1998). HRUs are the smallest units of the watershed in which relevant hydrologic components such as evapo-transpiration, surface ~~run-off~~runoff and peak rate of ~~run-off~~runoff, groundwater flow, and sediment yield can be estimated. Water balance is the driving force behind all of the processes in the SWAT calculated using eqn.~~n.~~ 7.

$$SW_t = SW_o + \sum_{I=1}^{t}\left(R_{day} - Q_{surf} - E_a - W_{seep} - Q_{gw}\right) \qquad (7)$$

where $SW_t$ is the final soil-water content (mm $H_2O$), $SW_o$ is the initial soil-water content on day i (mm $H_2O$), t is the time (days), $R_{day}$ is the amount of precipitation on day i (mm $H_2O$), $Q_{surf}$ is the amount of surface runoff on day i (mm $H_2O$), $E_a$ is the amount of evapo-transpiration on day i (mm $H_2O$), $W_{seep}$ is the amount of water entering the vadose zone from the soil profile on day i (mm $H_2O$), and $Q_{gw}$ is the amount of return flow on day i (mm $H_2O$).

Runoff is calculated separately for each HRU and routed to obtain the total streamflow for the watershed using either the soil conservation service (SCS) curve number (CN) method (Mockus, 1964) or Green & Ampt infiltration method (GAIM) (Green and Ampt, 1911) Figure 2. However, spatial connectivity and interactions among HRUs are ignored. Instead, the cumulative output of each spatially discontinuous HRU at the subwatershed outlet is directly routed to the channel (Pignotti et al., 2017). This lack of spatial connectivity among HRUs makes implementation and impact analysis of spatially-targeted management such as soil and water conservation structure difficult to incorporate into the model. Different authors have made efforts to overcome this problem— For instance, a grid-based version of the SWAT model (Rathjens et al., 2015), or landscape simulation on a regularized grid (Rathjens and Oppelt, 2012). Moreover, (Arnold et al., 2010) and (Bosch et al., 2010) further modified SWAT so that it allows landscapes to be subdivided into catenas comprising upland, hillslope, and floodplain units, and flow to be routed through these catenas. However, SWATgrid, developed to overcome this limitation, remains largely untested and computationally demanding (Rathjens et al., 2015).

Hence, the standard SWAT- CN method was chosen for this study because it is tested in many Ethiopian watersheds such as (Gashaw *et al.*, 2018; Gebremicael *et al.*, 2013; Setegn *et al.*, 2008; Woldesenbet *et al.*, 2017b). Furthermore, its ability to use daily input data (Arnold et al., 1998; Neitsch et al., 2011; Setegn et al., 2008) as compared to GAIM, which requires sub-daily precipitation as a model input, and that can be difficult to obtain in data-scare regions like the UBNRB. This study focused on the effects of LULC change and climate change on the basin's water balance components, which includes the components of inflows, outflows, and the change in storage. Precipitation is the main inflow, whereas evapo-transpiration (Et), surface runoff (Qs), lateral flow (Ql), and base flow (Qb) are the outflows. SWAT has three storages: soil moisture (SM), shallow aquifer (SA) and deep aquifer (DA). Water movement from the soil-moisture storage to the shallow aquifer is due to percolation, whereas water movement from the shallow aquifer reverse upward to the soil-moisture storage is Revap. For a more detailed description of the SWAT model, refer to Neitsch *et al.* (2011).

The SWAT model setup and data preparation can be done using arcSWAT tools in the arcGIS environment, whereas parameter sensitivity analysis, and model calibration and validation was performed using the SWAT-CUP (Calibration and Uncertainty Procedures) interface Sequential Uncertainty Fitting (SUFI-2) algorithm (Abbaspour, 2008). During model set up, the observed daily weather and streamflow data from the given period was divided in to three different periods; the

first to warm up the model, the second to calibrate it, ~~the model~~ and the third to validate it ~~the model~~. The first step in SWAT is to ~~he~~ determine ~~ation of~~ the most sensitive parameters for a given watershed using the global sensitivity analysis option (Arnold *et al.*, 2012). The second step is to complete the calibration process making necessary ~~adjusting~~ adjustments for the model's input parameters ~~necessary~~ to match model output with observed data, thereby reducing the prediction uncertainty. Initial parameter estimates were taken from the default lower and upper bound values of the SWAT model database and from earlier studies in the basin such as ~~e.g.~~ (Gebremicael *et al.*, 2013). The final step, model validation, involves running a model using parameters that were determined during the calibration process, and comparing the predictions to independently observed data not used in the calibration.

In this study, both manual and automatic calibration strategies were applied to attain the minimum differences between observed and simulated streamflows in terms of surface flow, and peak and total flow following the steps recommended by Arnold *et al.* (2012). For the purpose of impact analysis, we divided the simulation periods in ~~of~~ (1971–2010) into four decadal periods, hereafter referred as the 1970s (1971–1980), 1980s (1981–1990), 1990s (1991–2000) and 2000s (2001–2010), as shown in Table 2. The model's performance for the streamflow was then evaluated using statistical methods (Moriasi *et al.*, 2007) such as the Nash–Sutcliffe coefficient of efficiency (NSE), the coefficient of determination ($R^2$), and the relative volume error (RVE %), which are shown by eqn.8-10. Furthermore, graphical comparisons of the simulated and observed data, as well as water balance checks, were used to evaluate the model's performance.

$$R^2 = \frac{\left[\sum(Q_{m,i} - \bar{Q}_m)(Q_{s,i} - \bar{Q}_s)\right]^2}{\sum(Q_{m,i} - \bar{Q}_m)^2 \sum Q_{s,i} - \bar{Q}_s^2} \tag{8}$$

$$NSE = 1 - \frac{\sum(Q_m - Q_s)_i^2}{(Q_{m,i} - \bar{Q}_m)^2} \tag{9}$$

$$RVE\ (\%) = 100 * \frac{\sum_{i=1}^{n}(Q_m - Q_s)_i}{\sum_{i=1}^{n} Q_{m,i}} \tag{10}$$

where $Q_{m,i}$ is the measured streamflow in $m^3s^{-1}$, $\bar{Q}_m$ ~~$Q_m$~~ are ~~is~~ the mean values of the measured streamflow ($m^3s^{-1}$), $Q_{s,i}$ is the simulated streamflow in $m^3s^{-1}$, and $\bar{Q}_s$ ~~$Q_s$~~ are ~~is~~ the mean values of simulated data in $m^3s^{-1}$.

### 4.4 SWAT simulations

Three different approaches were ~~taken~~ applied ~~In order to~~ for assessing the individual and combined effects of LULC change and climate change on streamflow and water balance components, ~~three different approaches were applied~~. The first approach is to assess the response of streamflow to combined LULC change and climate change. We divided the analysis period, ~~(~~1971–2010,~~)~~ into four equal periods (four decades). These are, periods when land use changes are expected to change the hydrological regime within a catchment ~~is expected to be changed due to land use changes~~ (Marhaento *et al.*,

2017; Yin *et al.*, 2017b). The first period, the 1970s, was regarded as the baseline period. The other periods, the 1980s, 1990s, and 2000s, were regarded as altered periods. LULC maps of 1973, 1985, 1995, and 2010 were used to represent LULC patterns during the 1970s, 1980s, 1990s, and 2000s respectively. To analyze the response of streamflow and water balance components caused by the combined effects of LULC and climate change during decadal time periods, the SWAT model was separately calibrated and validated for each decade using the respective LULC map and weather data (Table 2). The DEM and soil data sets remained unchanged. The differences between the simulation result of the baseline and altered periods represent the combined effects of LULC and climate changes on streamflow and water balance components.

The second approach included simulations to attribute effects from LULC changes alone. It aimed to investigate whether LULC change is the main driver for changes in water balance components. To identify the hydrological impacts caused solely by LULC, "A fixing-changing" method was used (Marhaento *et al.*, 2017; Woldesenbet *et al.*, 2017b; Yan *et al.*, 2013; Yin *et al.*, 2017a). The calibrated and validated SWAT model and its parameter settings in the baseline period were forced by weather data from baseline period, 1973-1980, while changing only the LULC maps from 1985, 1995, and 2010, keeping the DEM and soil data constant as suggested by (Hassaballah *et al.*; Marhaento *et al.*, 2017; Woldesenbet *et al.*, 2017b; Yin *et al.*, 2017a). We ran the calibrated SWAT model for the baseline period (1970s) four times changing only the LULC map from the years 1973, 1985, 1995, and 2010 and remaining the constant weather data set from the 1970s (Table 2). The third approach is similar to the second but the simulations are attributed only for climate changes. A model was run again four times, corresponding to the LULC periods using a unique LULC map of the year 1973 but altering the four different periods of weather data sets (1970s, 1980s, 1990s, and 2000s).

## 5. Results and discussions

### 5.1 Trend test

#### 5.1.1 Rainfall

The summary of the MK trend-tests result for the rainfall recorded at the 15 selected stations located in and around the UBNRB revealed a mixed trend (increasing, decreasing, and no change). For daily time series, the computed probability values (p-values) for seven stations was greater, although for eight stations it was less, than the given significance level ($\alpha = 5$ %). This means that no statistically significant trends existed in seven stations, but a monotonic trend occurred in the remaining eight stations. Positive trends develop only at six stations, four of which were concentrated in the northern and central highlands (Bahirdar, Dangila, Debre Markos, and G/bet). The other two stations, Assosa and Angergutten, are located in the south-western and southern lowlands (see Figure 1). The other two stations,

Alemketema and Nedjo, which are located in the East and South-West of the UBNRB, respectively showed a decreasing trend. On monthly basis, the MK trend test result showed that no statistically significant trend existed in all 15 stations. On an annual time scale, MK trend test could not find any trend in 11 stations, although the (Alemketema, Debiremarkos, Gimijabet, and Shambu stations) did exhibit a trend. The trend analysis result for the annual rainfall time series agrees well with a previous study by Gebremicael *et al.* (2013), who reported no significant annual rainfall change at eight out of nine stations during the 1973–2005 period. Hence, it is interesting to note that the time scale of analysis is critical factor in determining the given trends.

The basin-wide rainfall trend and change point analysis was again carried out on daily, monthly, seasonal, and annual time scales using the MK and Pettitt tests respectively, as summarized in Table 3 and Figure 3. The MK test showed increasing trends for annual, monthly, and long-rainy-season rainfall series whereas no trend for daily, short rainy, and dry-season rainfall series appeared. The magnitude of trends for annual, monthly, and long-rainy-season rainfall series are not significant, as explained by the values of Sen's slope. However, the Pettitt test could not detect any jump point in basin-wide rainfall series except for daily time-series rainfall (see Figure S01).

Previous studies' authors, such as (Conway, 2000; Gebremicael *et al.*, 2013; Tesemma *et al.*, 2010), conducted the trend analysis of basin-wide rainfall and reported that no significant change in annual and seasonal rainfall series across the UBNRB which contradicts with the result of this study. This disagreement could be due to the number of stations and their spatial distribution across the basin, time period of the analysis, approach used to calculate basin-wide rainfall from gauging stations, and data sources. Tesemma et al. (2010) used monthly rainfall data downloaded from Global Historical Climatology Network (GHCN) data base and 10-day rainfall data for the 10 selected stations obtained from the National Meteorological Service Agency of Ethiopia from 1963–2003. Conway (2000) also constructed basin-wide annual rainfall in the UBNRB for the 1900–1998 period from the mean of 11 gauges. Furthermore, (Conway, 2000) employed simple linear regressions over time to detect trends in annual rainfall series without removing the serial autocorrelation effects. Gebremicael *et al.* (2013), also used only nine stations from the 1970–2005 period. However, in this study, we used daily observed rainfall data from 15 stations collected from Ethiopian Meteorological Agency from 1971–2010. The stations are more or less evenly spatially distributed over the UBNRB. We applied a widely used spatial interpolation technique, the Thiessen polygon method, to calculate basin-wide rainfall series from station data.

**5.1.2 Streamflow**

The MK test's result for daily, monthly, annual, and seasonal (long and short rainy season and dry season) time-series streamflow showed a positive trend, the magnitude of which is statistically significant, as summarised

summarized in Table 3. Meanwhile, although the Pettitt test detects change point for daily, annual, and short-rainy-season streamflows, it cannot detect change point for monthly, long, and dry season streamflows (see Figure 3 and Figure S02). The change point detected by the Pettitt test for annual rainfall series occurred in 1995 whereas for daily and dry seasons it are respectively in 1985 and 1987. The result obtained from the MK test agrees well with the previous study conducted by Gebremicael et al. (2013), which reported an increasing trend in the observed annual, short, and long rain seasons' streamflow at the El Diem gauging station, but disagrees with the result for dry-season streamflow. Furthermore, the increasing trend of long-rainy-season streamflow agrees well with the result of Tesemma et al. (2010), but disagrees with the results of short rainy season and annual flows. (Tesemma *et al.*, 2010), reported that the short rainy season and the annual flows are constant for the 1964–2003 period analyzed. This disagreement is likely attributable to the difference in analysis period, as can be seen from Figure 3. The last seven years (2004–2010) had relatively higher streamflow records.

Although, the results of MK test for annual and long-rainy-season rainfall and streamflow show an increasing trend for the last 40 years in the UBNRB, the magnitude of Sen's slope for streamflow is much larger than it is for rainfall (Table 3). Moreover, short-rainy-season streamflow shows a statistically significant positive increase whereas the rainfall shows no change. The mismatch between rainfall and streamflow trend magnitude could be associated with evapotranspiration and attributable to the combined effect of LULC change and climate change, infiltration rate due to changing soil properties, rainfall intensity, and extreme events.

## 5.2 LULC change analysis

According to the confusion-matrix report, overall accuracy of 80 %, producer's accuracy values for all classes ranged from 75.4 % to 100 %, user's accuracy values ranging from 83.7 % to 91.7 % and a kappa coefficient (k) of 0.77 were attained for the 2010 classified image, as shown in Table 5. Monserud (1990) suggested a kappa value of <40 % as poor, 40–55 % fair, 55–70 % good, 70–85 % very good, and >85 % as excellent. According to these ranges, the classification in this study has very good agreement with the validation data set and met the minimum accuracy requirements to be used for further change detection and impact analysis.

The classified images of the basin (Figure 4) have shown different LULC proportions at four distinct time periods, as shown in Figure 5. Cultivated land dominantly covers (62.9 %) of UBNRB, followed by bushes and shrubs (18 %), forest (17.4 %), and water (1.74 %) in 1973. In 1985, cultivated land area increased to 65.6 %, followed by bushes and shrubs (18.3 %), while forest decreased to 14.4 %, and water remained unchanged at 1.7 %. In 1995, cultivated land area further increased to 67.5 %, followed by bushes and shrubs (18.5 %). Forest further decreased to 12.2 %, and water remained unchanged at 1.7 %. In 2010,

cultivated land decreased to 63.9 %, bushes and shrubs increased to 18.8 %, forest increased to 15.6 %, and water remained unchanged at 1.7 %. During the entire 1973–2010 period, cultivated land, along with bushes and shrubs remained the major proportions compared to the other LULC classes. The highest gain (2.7 %) and the largest loss (-3.6 %) in cultivated land occurred during the 1973–1985 and 1995–2010 periods respectively. The highest gain in bushes and shrubs was 0.3 % from 1973 to 1985, whereas the highest gain in forest coverage (3.4 %) was recorded during the 1995–2010 period. Water coverage remained unchanged from 1973 to 2010.

Although, the image classification enjoys very good accuracy, uncertainties could be expected for the following reasons. Firstly, as elsewhere in Ethiopia, LULCs change rapidly over the land surface of the basin, and image reflectance may be confusing due to the topography and variation in the image acquisition date. Landsat images were not all available for one particular year or one season; images thus came from a mix of years, and a variety of seasons might harbor errors. Secondly, the workflow associated with LULC classification involves many steps and can be a source of uncertainty. The errors are observed in the classified LULC map as shown in Figure 4. On the western side of the map in Figure 4 (a) a rectangular section with forest appears, which completely disappears in 4(b). A rectangular forest cover appears in the northern part of the country in 4(b), which again disappears completely in 4(c). In 4(d), forest cover with linear edges (North-South) appears on the map's eastern side. That being recognized, the land-cover mapping is reasonably accurate overall, providing a good base for land-cover estimation and for providing basic information for hydrological impact analysis.

The rate of expansion of cultivated land before 1995 was higher than that after 1995. Conversely, the area devoted to forest land decreased in 1985 and 1995 from the 1973 baseline. However, after 1995, the forest's size began to increase while the amount of cultivated land decreased. The increased forest coverage and the reduction in cultivated land over the period 1995 to 2010 showed that the environment was recovering from the devastating drought, and forest clearing for firewood and cultivation due to population growth has been minimized. This could be due to the afforestation program, which the Ethiopian government initiated, and to the extensive soil and water conservation measures carried out by the community. Since 1995, eucalyptus tree plantation expanded significantly across the country at homestead level for fire wood, construction material, charcoal production, and income generation (Woldesenbet *et al.*, 2017b). In summary, forest coverage declined by 1.8 %, while both bushes and shrubs as well as cultivated land increased by 0.8 % and 1 % respectively during the 2010 period from the original 1973 level. This result agrees well with other studies (Gebremicael *et al.*, 2013; Rientjes *et al.*, 2011; Teferi *et al.*, 2013; Woldesenbet *et al.*, 2017b), who reported a significant conversion of natural vegetation cover into agricultural land.

## 5.3 SWAT model calibration and validation

The SWAT model's most sensitive parameters for simulating streamflow were identified using global sensitivity analysis of SWAT-CUP. Their optimized values were determined by the calibration process that Arnold *et al.* (2012) recommended. Parameters such as SCS curve number (CN2), base flow alpha factor (ALPHA_BF), soil evaporation compensation factor (ESCO), threshold water depth in the shallow aquifer required for return flow to occur (GWQMN), groundwater "revap" coefficient (GW_REVAP), and available water capacity (SOL_AWC) were found to be the most sensitive parameters for the flow predictions.

Figure 6 shows the calibration and the validation results for monthly streamflow hydrographs. These results revealed that the model captured the monthly hydrographs well. The $R^2$, NSE, and RVE (%) statistical performance measures, as presented in Table 6, reverified this. For the calibration period, the values of $R^2$, NSE, and RVE (%) from the four model ranged from 0.79 to 0.91, 0.74 to 0.91, and −3.4 % to 4 %. For the validation period they ranged from 0.84 to 0.94, 0.82 to 0.92, and −7.5 % to 7.2 % respectively. According to the rating of Moriasi *et al.* (2007), the SWAT model's performance over the UBNRB can be categorized as very good, although underestimation was observed in the base-flow simulation. The optimal parameter values of the four calibrated model runs are shown in Table 7. A change was obtained for CN2 parameter values, which can be attributed to the catchment's response behaviour. For instance, an increase in the CN2 value in the 1980s and 1990s from 0.88 to 0.91 and 0.92 compared to the 1970s respectively, indicate a reduction in forest coverage and expansion of cultivated land. In contrary, a decrease in CN2 value was attained during the period 1990s to 2000s from 0.92 to 0.9, attributed to the increase in forest coverage and reduction in cultivated land.

## 5.4 Combined Effects of LULC change and climate change on streamflow and water balance components

The simulation results of the four independent, decadal-time-scale calibrated and validated SWAT model runs reflect the combined effect of both LULC and climate change during the past 40 years' (Table 8). From the simulation result, mean annual streamflow increased by 16.9 % between the 1970s and the 2000s. However, the rate of change is different in different decades. For example, it increased by 3.4 % and 9.9 % during the 1980s and 1990s respectively from the baseline 1970s period.

The ratio of mean annual streamflow to mean annual precipitation (Qt/P) increased from 19.4 % to 22.1 %, and actual evaporation to precipitation (Ea/P) decreased from 61.1 % to 60.5 % from the 1970s to 2000s. Moreover, the ratio of surface runoff to streamflow (Qs/Qt) has increased significantly from 40.7 % in the 1970s to 50.1 % and 55.4 % in the 1980s and 1990s respectively, and decreased to 43.7 % in the 2000s. In contrast, the base flow to streamflow ratio (Qb/Qt) has significantly decreased from 17.1 % in the 1970s to 10.3 % and 3.2 % respectively during the

1980s and 1990s, but has increased to 20 % in the 2000s. The result for surface runoff agrees with the previous study done by (Gebremicael *et al.*, 2013), but disagrees for baseflow. They reported surface runoff ($Q_s$) contribution to the total river discharge has increased by 75%, while the baseflow ($Q_b$) flow has decreased by 50% from the 1970s to 2000s.

In general, 1.8 % forest cover loss and 1 % increased cultivated land combined with 2.2 % increased rainfall from the 1970s to the 2000s led to a 16.9 % increase in simulated streamflow. The 1990s was the period during which the highest deforestation and expansion of cultivated land was reported; meanwhile, it is the time when the rainfall intensity and the number of rainfall events have significantly increased compared to the 1970s and 1980s, as shown in Table 4. Hence, the increased mean annual streamflow could be ascribed to the combined effects of LULC and climate change. In the case of ($Q_s/Q_t$), the increasing pattern could be ascribed to increasing rainfall intensities and the expansion of cultivated land and diminution of forest coverage, which might adversely affect soil water storage and decrease rainfall infiltration, thereby increasing water yield or streamflow. In contrast, the decreasing ($Q_b/Q_t$) is positively related with the increasing evapotranspiration linked to both LULC and climate factors (Table 8). This hypothesis can be explained with the change in CN2 parameter values obtained during calibration of the four SWAT model runs.

The CN2 parameter value —which is a function of evapotranspiration derived from LULC, soil type, and slope—, increased in the 1980s and 1990s relative to the 1970s, and could be associated with the expansion of cultivated land and shrinkage of forest land. The increasing CN2 results reflect more surface runoff and less baseflow being generated.

Another important factor contributing to decreasing of surface runoff and increasing base flow ration from 1990s to the 2000s could be the establishment of soil and water conservation (SWC) measures. According to Haregeweyn et al. (2015), various nationwide SWC initiatives such as Food-for-Work (FFW), Managing Environmental Resources to Enable Transition (MERET) to more sustainable livelihoods, Productive Safety Net Programs (PSNP), Community Mobilization through free-labor days, and the National Sustainable Land Management Project (SLMP) have been undertaken since the 1980s. (Haregeweyn *et al.*, 2015) evaluated these initiatives' effectiveness and concluded that community labour mobilization seems to be the best approach. This can reduce mean seasonal surface runoff by 40 %, with broad spatial variability ranging from 4 % in Andit Tid (northwest Ethiopia) to 62 % in Gununo (south Ethiopia).

**5.5 Effects of an isolated LULC change on streamflow and water balance components**

(Yan *et al.*, 2013) used "A fixing -changing" method to identify the hydrological impacts of LULC alone. The calibrated and validated SWAT model and its parameter settings in the baseline period was forced by weather data from the baseline 1973-1980 period while changing only the LULC maps from 1985, 1995, and 2010, keeping the DEM and soil data constant as suggested by (Hassaballah *et al.*). The result from Figure 7 indicated that Qs/Qt ratio changed from 40.7 % to 41.2 %, 41.1 %, and 40.9 % respectively by using the LULC maps from 1973, 1985, 1995 and 2010 whereas the Qb/Qt ratio changed from 17.1 % to 16.8 %, 16.5 %, and 16.9 % respectively. The highest Qs/Qt ratio (41.9 %) and the lowest Qb/Qt ratio (16.5 %) were recorded with the 1995 LULC map. This could be attributed to the 5.1 % reduction in forest coverage and 4.6 % increase in cultivated land with the 1995 LULC map relative to the 1973 LULC map.

On a basin scale, over a decadal time period, water gains mainly from precipitation. The losses are mainly due to runoff and evapotranspiration (Oki *et al.*, 2006). With the fixing-changing approach, the change in streamflow attribiutable to LULC change was essentially the change in evapotranspiration between the two periods, as the amount of precipitation was constant (1970s) and the change in water storage during the two periods was similar (Yan et al., 2013). Annual Ea losses from seasonal crops are smaller than those from forests, because seasonal crops transpire during a relatively shorter time interval than perennial trees (Yan et al., 2013). As a result, the actual mean annual evapotranspiration (Ea) simulated by the SWAT model was 871.6 mm at the baseline. It decreased to 871.4 mm and 871 mm in 1985 and 1995 respectively and increased to 872.1 mm in 2010. This could be due to simultaneous expansion of cultivated land and shrinkage in forest coverage in the 1985 and 1995 LULC maps relative to the 1973 base line. Furthermore, this deforestation may reduce canopy interception of the rainfall, decreases soil infiltration by increasing raindrop impacts, and reducing plant transpiration, which can significantly increase surface runoff and reducing base flow (Huang et al., 2013). Here, the evapotranspiration change caused by the LULC change is minimal. as a result, the change for surface runoff and baseflow is not significant.

**5.6 Effects of isolated climate change on streamflow and water balance components**

The impacts of climate change are analyzed by running the four models using a unique LULC map of 1973 with its model parameters while changing only the weather data sets from 1970s, 1980s, 1990s, and 2000s. The simulated water balance components shown in Figure 7, indicate that the Qs/Qt ratio increased from 40.7 % to 45.2 %, 45.6 %, and 46.2 % during the 1970s, 1980s, 1990s and 2000s respectively, while the Qb/Qt ratio changed from 17.1 % to 13.5 %, 14.9 %, and 12.7 % for the same simulation

periods. The decreasing (Qb/Qt) ratio for the altered periods compared to the baseline period could be attributed to evapotranspiration increasing from 872 mm to 854 mm, 906 mm, and 884 mm respectively in 1970s, 1980s, 1990s, and 2000s, which can be linked to temperature and amount of rainfall. However, it is important to know the dominant rainfall-runoff process in the study area to fully understand the effect of climate change on the water balance components.

Although, no detailed research has been conducted on the Blue Nile basin to investigate the runoff generation processes, Liu et al. (2008) investigated the rainfall-runoff processes at three small watersheds located inside and around Upper Blue Nile basin, namely, Mayber, AnditTid, and Anjeni. Their analysis showed that, unlike in temperate watersheds, in monsoonal climates, a given rainfall volume at the onset of the monsoon produces a different runoff volume than the same rainfall at the end of the monsoon. Liu et al. (2008) and Steenhuis et al. (2009) showed that the ratio of discharge to precipitation minus evapotranspiration, $Q/(P - ET)$, increases with cumulative precipitation from the onset of monsoon. This suggests that saturation excess processes play an important role in watershed response.

Furthermore, the infiltration rates that Engda (2009) measured in 2008 were compared with rainfall intensities in the Maybar and Andit Tid watersheds located inside and around the UBNRB. In the Andit Tid watershed, which has an area of less than 500 ha, the measured infiltration rates at 10 locations were compared with rainfall intensities considered from the 1986 – 2004 period. The analysis showed that only 7.8 % of rainfall intensities were found to be higher than the lowest soil infiltration rate of 2.5 cm hr$^{-1}$. Derib (2005) performed a similar analysis in the Maybar watershed (with a catchment area of 113 ha). The infiltration rates measured from 16 measurements ranged from 19 mm h$^{-1}$ to 600 mm hr$^{-1}$ with a 24 cm hr$^{-1}$ average and 18 cm hr$^{-1}$ median whereas the average daily rainfall intensity from 1996 to 2004 was 8.5 mm hr$^{-1}$. Hence, he suggested from these infiltration measurements that infiltration excess runoff is not a common feature in these watersheds.

From the above discussion points, it is to be noted that surface runoff could increase with increasing total rainfall amount regardless of rainfall intensity. However, the mean annual rainfall amount in this study was decreasing from the 1970s to the 1980s (1428 mm and 1397 mm respectively) while the (Qs/Qt) ratio increased from 40.7 % to 45.2 %. Similarly, the mean annual rainfall amount in the 1990s (1522 mm) was higher than the mean annual rainfall amount in the 2000s (1462 mm) while the (Qs/Qt) increased from 45.6 % to 46.2 %. In contrast, climate indexes such as 99-percentile rainfall, SDII (ratio of total precipitation amount to R1mm), and R20mm are increasing consistently from 1970 to the 2000s, as shown in Table 4. This indicates that the increasing of surface runoff might be due to an increasing of number of extreme rainfall events and rainfall intensity. In other words, this study revealed that infiltration excess of overland flow dominates the rainfall-runoff processes in the UBNRB, not saturation excess of

overland flow. The contradiction from the previous studies might be due either to the limitation of the SWAT-CN method when applied in monsoonal climates or the overlooked of tillage activities, which significantly impact the soil infiltration rate. Extensive tillage activities are carried out across the basin at the beginning of the rainy season. Soils get disturbed as a result, which can increase the infiltration rate and ultimately decrease the amount of rainfall converted to runoff.

Although, the CN method is easy to use and provides acceptable results for discharge at the watershed outlet in many cases, researchers have concerns about its use in watershed models (Steenhuis et al., 1995; White et al., 2011). The SWAT-CN model relies with a statistical relationship between soil moisture condition and CN value obtained from plot data in the United States with a temperate climate that was never tested in a monsoonal climate exhibiting two extreme soil moisture conditions. In monsoonal climates, long periods of rain can lead to prolonged soil saturation whereas during the dry period, the soil dries out completely, which may not happen in temperate climates (Steenhuis *et al.*, 2009). Hence, further research that considers bio-physical activities such as tillage and seasonal effects on soil moisture at representative watersheds of the basin is necessary for properly assessing the rainfall-runoff processes.

**6. Conclusions**

This study's objectives were to understand the long-term variations of rainfall and streamflow of the UBNRB using statistical techniques (MK and Pettitt tests) and to assess the combined and isolated effects of climate and LULC change using a semi-distributed hydrological model (SWAT). Although the results of the MK test for annual and long-rainy-season rainfall and streamflow show an increasing trend in the UBNRB for the last 40 years, the magnitude of Sen's slope for streamflow is much larger than the Sen's slope of areal rainfall. Moreover, for the short-rainy-season streamflow shows a statistically significant positive increase while the rainfall shows no change. The mismatch of trend magnitude between rainfall and streamflow could be attributed to the combined effect of LULC and climate change, associated with decreasing actual evapotranspiration (Ea) and increasing rainfall intensity and extreme events.

LULC change detection was assessed by comparing the classified images. The result showed that the dominant process is largely the expansion of cultivated land and decrease in forest coverage. The rate of deforestation is high during the 1973–1995 period. This is probably due to the severe drought that occurred in the mid-1980s and a large population increase resulting from the expansion of agricultural land. On the other hand, forest coverage increased by 3.4 % during the period 1995 to 2010. This indicates that the environment was recovering from the devastating drought of

in the 1980s, regenerating of forests as the result of afforestation program initiated by the Ethiopian government, and due to soil and water conservation activities accomplished by the communities.

The SWAT model was used to analyze the combined and isolated effects of LULC and climate changes on the monthly streamflow at the basin outlet (El Diem station, located on the Ethiopia-Sudan border). The result showed that the combined effects of the LULC and climate changes increased the mean annual streamflow by 16.9 % from the 1970s to the 2000s. The increased mean annual streamflow could be ascribed to the combined effects of LULC and climate change. The LULC change alters the catchment responses. As a result, SWAT model parameter values could be changed. For instance, the expansion of cultivation land and the shrinkage of forest coverage from 1973 to 1995 changed the CN2 parameter's values from 0.89 in 1973 to 0.91 and 0.92 in 1985 and 1995 respectively. Increasing of CN2 value might increase surface runoff and decrease base flow. Similarly, the increase in rainfall intensity and extreme precipitation events led to a substantial increase in Qs/Qt, a substantial decrease in Qb/Qt, and ultimately to increases in the streamflow during the 1971–2010 simulation period.

The "fixing-changing" approach result using the SWAT model revealed that the isolated effect of LULC change could potentially alter the streamflow generation processes. Expansion of cultivated land might reduce evapotranspiration because seasonal crops transpire less than perennial trees do (Yan et al., 2013) resulting in increased surface runoff. Alternatively, reduction of forest coverage may reduce canopy interception of the rainfall, decrease the soil infiltration by increasing raindrop impacts, and reduce plant transpiration, which can significantly increase surface runoff and reduce base-flow (Huang et al., 2013). In general, a 5.1 % reduction in forest coverage and a 4.6 % increase in cultivated land led to a 9.9 % increase in mean annual streamflow from 1973 to 1995. This study provides a better understanding and substantial information about how climate and LULC change affects streamflow and water balance components separately and jointly, which is useful for basin-wide water resources management. The SWAT simulation indicated that the impacts of climate change are more substantial than the impacts of LULC change, as shown in Figure 7. Surface water is no longer used for agriculture and plant consumption in areas such as the UBNRB, where water-storage facilities are scarce. On the other hand, base flow provides the most reliable source for the irrigation needed to increase agricultural production. Hence, the increasing amount of surface water and diminished base flow caused by both LULC and climate changes negatively affect socio-economic developments in the basin.

Therefore, protecting and conserving the natural forests and expanding soil and water conservation activities is therefore highly recommended, not only for increasing the base flow available for irrigation but also to reduce soil erosion. By doing so, the might increase productivity, and livelihoods as well as regional water resource use cooperation might improve. However, the uncertainties of Landsat

image classification and the SWAT-model simulation might limit this study of SWAT model. TIn order to improve the accuracy of LULC classification from Landsat images, further efforts such as the integratingon of other images together with Landsat images through image-fusion techniques (Ghassemian, 2016) areis required. The SWAT model does not adjust CN2 for slopes greater than 5%., Thiswhich could be significant in areas where the majority of the area has a slope greater than 5%, such as in the UBNRB. WTherefore, we therefore suggest adjusting the CN2 values for slope >-5 % outside of the SWAT model might improve the results. Moreover, further research that involvinges rainfall intensity, infiltration rate, and event-based analysis of hydrographs and critical evaluation of rainfall-runoff processes in the study area might overcomeimprove this study'se limitations of this study. Finally, the authors would like to point out that the impacts of current and future water resource developments should be investigated in order to establish comprehensive, and holistic water resource management in the Nile basin.

Acknowledgements. The authors would like to thank the Ethiopian Ministry of Water, Irrigation and Electricity and the Ethiopian National Meteorological Services Agency for providing the streamflow and meteorological data, respectively for free. The authors would also like to express their gratitude to the anonymous referees and the editor, Prof. Axel Bronstert, who gave constructive remarks and comments for enhancing the quality of the manuscript.

## References

Abbaspour, C.K., 2008. SWAT Calibrating and Uncertainty Programs. A User Manual. Eawag Zurich, Switzerland.

Allen, R.G., Pereira, L.S., Raes, D., Smith, M., 1998. Crop evapotranspiration-Guidelines for computing crop water requirements-FAO Irrigation and drainage paper 56. FAO, Rome, 300(9): D05109.

Arnold, J., Allen, P., Volk, M., Williams, J., Bosch, D., 2010. Assessment of different representations of spatial variability on SWAT model performance. Transactions of the ASABE, 53(5): 1433-1443.

Arnold, J.G., Moriasi, D.N., Gassman, P.W., Abbaspour, K.C., White, M.J., Srinivasan, R., Santhi, C., Harmel, R., Van Griensven, A., Van Liew, M.W., 2012. SWAT: Model use, calibration, and validation. Transactions of the ASABE, 55(4): 1491-1508.

Arnold, J.G., Srinivasan, R., Muttiah, R.S., Williams, J.R., 1998. Large area hydrologic modeling and assessment part I: Model development1. Wiley Online Library.

Awulachew, S.B., McCartney, M., Steenhuis, T.S., Ahmed, A.A., 2009. A review of hydrology, sediment and water resource use in the Blue Nile Basin, 131. IWMI.

Banko, G., 1998. A review of assessing the accuracy of classifications of remotely sensed data and of methods including remote sensing data in forest inventory.

BCEOM, 1998. Abbay river basin integrated development master plan project, phase 3 main report. Ministry of Water Resources, Addis Ababa, Ethiopia, Volume I, Main report.

Bewket, W., Sterk, G., 2005. Dynamics in land cover and its effect on stream flow in the Chemoga watershed, Blue Nile basin, Ethiopia. Hydrological Processes, 19(2): 445-458.

Bosch, D., Arnold, J., Volk, M., Allen, P., 2010. Simulation of a low-gradient coastal plain watershed using the SWAT landscape model. Transactions of the ASABE, 53(5): 1445-1456.

Cheung, W.H., Senay, G.B., Singh, A., 2008. Trends and spatial distribution of annual and seasonal rainfall in Ethiopia. International Journal of Climatology, 28(13): 1723-1734.

Congalton, R.G., 1991. A review of assessing the accuracy of classifications of remotely sensed data. Remote sensing of environment, 37(1): 35-46.

Conway, D., 2000. The climate and hydrology of the Upper Blue Nile River. The Geographical Journal, 166(1): 49-62.

DeFries, R., Chan, J.C.-W., 2000. Multiple criteria for evaluating machine learning algorithms for land cover classification from satellite data. Remote Sensing of Environment, 74(3): 503-515.

Derib, S.D., 2005. Rainfall-runoff processes at a hill-slope watershed: case of simple models evaluation at Kori-Sheleko Catchments of Wollo, Ethiopia, M. Sc. Thesis.

Engda, T.A., 2009. Modeling rainfall, runoff and soil loss relationships in the northeastern highlands of Ethiopia, andit tid watershed, Citeseer.

Gashaw, T., Tulu, T., Argaw, M., Worqlul, A.W., 2018. Modeling the hydrological impacts of land use/land cover changes in the Andassa watershed, Blue Nile Basin, Ethiopia. Science of The Total Environment, 619: 1394-1408.

Gebremicael, T., Mohamed, Y., Betrie, G., van der Zaag, P., Teferi, E., 2013. Trend analysis of runoff and sediment fluxes in the Upper Blue Nile basin: A combined analysis of statistical tests, physically-based models and landuse maps. Journal of Hydrology, 482: 57-68.

Ghassemian, H., 2016. A review of remote sensing image fusion methods. Information Fusion, 32: 75-89.

Green, W.H., Ampt, G., 1911. Studies on Soil Phyics. The Journal of Agricultural Science, 4(01): 1-24.

Hamed, K.H., Rao, A.R., 1998. A modified Mann-Kendall trend test for autocorrelated data. Journal of Hydrology, 204(1-4): 182-196.

Haregeweyn, N., Tsunekawa, A., Nyssen, J., Poesen, J., Tsubo, M., Tsegaye Meshesha, D., Schütt, B., Adgo, E., Tegegne, F., 2015. Soil erosion and conservation in Ethiopia: a review. Progress in Physical Geography, 39(6): 750-774.

Hassaballah, K., Mohamed, Y., Uhlenbrook, S., Biro, K., Analysis of streamflow response to land use land cover changes using satellite data and hydrological modelling: case study of Dinder and Rahad tributaries of the Blue Nile (Ethiopia/Sudan).

Hayes, D.J., Sader, S.A., 2001. Comparison of change-detection techniques for monitoring tropical forest clearing and vegetation regrowth in a time series. Photogrammetric engineering and remote sensing, 67(9): 1067-1075.

Hu, Y., De Jong, S., Sluiter, R., 2004. A modeling-based threshold approach to derive change/no change information over vegetation area, Proceedings of the "12 International Conference on Geoinformatics-Geospatial Information Research: Bridging the Pacific and Atlantic". University of Gävle (Sweden), pp. 647-654.

Huang, J., Wu, P., Zhao, X., 2013. Effects of rainfall intensity, underlying surface and slope gradient on soil infiltration under simulated rainfall experiments. Catena, 104: 93-102.

Jensen, J.R., 1996. Introductory digital image processing: a remote sensing perspective. Prentice-Hall Inc.

Kendall, M., 1975. Rank correlation methods.

Liu, B.M., Collick, A.S., Zeleke, G., Adgo, E., Easton, Z.M., Steenhuis, T.S., 2008. Rainfall-discharge relationships for a monsoonal climate in the Ethiopian highlands. Hydrological Processes, 22(7): 1059-1067.

Lu, D., Mausel, P., Batistella, M., Moran, E., 2004. Comparison of land-cover classification methods in the Brazilian Amazon Basin. Photogrammetric engineering & remote sensing, 70(6): 723-731.

Mancino, G., Nolè, A., Ripullone, F., Ferrara, A., 2014. Landsat TM imagery and NDVI differencing to detect vegetation change: assessing natural forest expansion in Basilicata, southern Italy. iForest-Biogeosciences and Forestry, 7(2): 75.

Mann, H.B., 1945. Nonparametric Tests Against Trend. Econometrica, 13(3): 245-259.

Marhaento, H., Booij, M.J., Rientjes, T., Hoekstra, A.Y., 2017. Attribution of changes in the water balance of a tropical catchment to land use change using the SWAT model. Hydrological Processes, 31(11): 2029-2040.

McCartney, M., Alemayehu, T., Easton, Z.M., Awulachew, S.B., 2012. Simulating current and future water resources development in the Blue Nile River Basin. The Nile River Basin: water, agriculture, governance and livelihoods. Routledge-Earthscan, Abingdon: 269-291.

Mekonnen, D.F., Disse, M., 2018. Analyzing the future climate change of Upper Blue Nile River basin using statistical downscaling techniques. Hydrology and Earth System Sciences, 22(4): 2391.

Melesse, A., Abtew, W., Dessalegne, T., Wang, X., 2009. Low and high flow analyses and wavelet application for characterization of the Blue Nile River system. Hydrological processes, 24(3): 241.

Mengistu, D., Bewket, W., Lal, R., 2014. Recent spatiotemporal temperature and rainfall variability and trends over the Upper Blue Nile River Basin, Ethiopia. International Journal of Climatology, 34(7): 2278-2292.

Mockus, V., 1964. National engineering handbook,Section 4:Hydrology, 630.

Monserud, R.A., 1990. Methods for comparing global vegetation maps.

Moriasi, D.N., Arnold, J.G., Van Liew, M.W., Bingner, R.L., Harmel, R.D., Veith, T.L., 2007. Model evaluation guidelines for systematic quantification of accuracy in watershed simulations. Trans. Asabe, 50(3): 885-900.

Neitsch, S., Arnold, J., Kiniry, J.e.a., Srinivasan, R., Williams, J., 2002. Soil and water assessment tool user's manual version 2000. GSWRL report, 202(02-06).

Neitsch, S.L., Arnold, J.G., Kiniry, J.R., Williams, J.R., 2011. Soil and water assessment tool theoretical documentation version 2009, Texas Water Resources Institute.

NMA, 2013. Annual climate buletien for the year 2013. National Meteorological Agency, Meteorological Data and Climatology Directorate, Addis Ababa, Ethiopia, http://www.ethiomet.gov.et/bulletins/bulletin_viewer/bulletins/348/2013_Annual_Bulletin/en.

Oki, T., Kanae, S., 2006. Global hydrological cycles and world water resources. science, 313(5790): 1068-1072.

Pettitt, A., 1979. A non-parametric approach to the change-point problem. Applied statistics: 126-135.

Pignotti, G., Rathjens, H., Cibin, R., Chaubey, I., Crawford, M., 2017. Comparative Analysis of HRU and Grid-Based SWAT Models. Water, 9(4): 272.

Polanco, E.I., Fleifle, A., Ludwig, R., Disse, M., 2017. Improving SWAT model performance in the upper Blue Nile Basin using meteorological data integration and subcatchment discretization. Hydrology and Earth System Sciences, 21(9): 4907.

Rathjens, H., Oppelt, N., 2012. SWATgrid: An interface for setting up SWAT in a grid-based discretization scheme. Computers & geosciences, 45: 161-167.

Rathjens, H., Oppelt, N., Bosch, D., Arnold, J.G., Volk, M., 2015. Development of a grid-based version of the SWAT landscape model. Hydrological processes, 29(6): 900-914.

Rientjes, T., Haile, A., Kebede, E., Mannaerts, C., Habib, E., Steenhuis, T., 2011. Changes in land cover, rainfall and stream flow in Upper Gilgel Abbay catchment, Blue Nile basin-Ethiopia. Hydrology and Earth System Sciences, 15(6): 1979.

Seleshi, Y., Zanke, U., 2004. Recent changes in rainfall and rainy days in Ethiopia. International journal of climatology, 24(8): 973-983.

Sen, P.K., 1968. Estimates of the regression coefficient based on Kendall's tau. Journal of the American statistical association, 63(324): 1379-1389.

Setegn, S.G., Srinivasan, R., Dargahi, B., 2008. Hydrological modelling in the Lake Tana Basin, Ethiopia using SWAT model. The Open Hydrology Journal, 2(1).

Singb, A., 1989. Digital change detection techniques using remotelyWsensed data. International Journal of Remote Sensing, 10(6): 989L1003.

Singh, A., 1989. Review article digital change detection techniques using remotely-sensed data. International journal of remote sensing, 10(6): 989-1003.

Steenhuis, T.S., Collick, A.S., Easton, Z.M., Leggesse, E.S., Bayabil, H.K., White, E.D., Awulachew, S.B., Adgo, E., Ahmed, A.A., 2009. Predicting discharge and sediment for the Abay (Blue Nile) with a simple model. Hydrological processes, 23(26): 3728-3737.

Steenhuis, T.S., Winchell, M., Rossing, J., Zollweg, J.A., Walter, M.F., 1995. SCS runoff equation revisited for variable-source runoff areas. Journal of Irrigation and Drainage Engineering, 121(3): 234-238.

Teferi, E., Bewket, W., Uhlenbrook, S., Wenninger, J., 2013. Understanding recent land use and land cover dynamics in the source region of the Upper Blue Nile, Ethiopia: Spatially explicit statistical modeling of systematic transitions. Agriculture, ecosystems & environment, 165: 98-117.

Tekleab, S., Mohamed, Y., Uhlenbrook, S., Wenninger, J., 2014. Hydrologic responses to land cover change: the case of Jedeb mesoscale catchment, Abay/Upper Blue Nile basin, Ethiopia. Hydrological Processes, 28(20): 5149-5161.

Tesemma, Z.K., Mohamed, Y.A., Steenhuis, T.S., 2010. Trends in rainfall and runoff in the Blue Nile Basin: 1964–2003. Hydrological processes, 24(25): 3747-3758.

Uhlenbrook, S., Mohamed, Y., Gragne, A., 2010. Analyzing catchment behavior through catchment modeling in the Gilgel Abay, upper Blue Nile River basin, Ethiopia. Hydrology and Earth System Sciences, 14(10): 2153-2165.

von Storch, H., 1995. Misuses of Statistical Analysis in Climate Research, Analysis of Climate Variability. Springer, pp. 11-26.

White, E.D., Easton, Z.M., Fuka, D.R., Collick, A.S., Adgo, E., McCartney, M., Awulachew, S.B., Selassie, Y.G., Steenhuis, T.S., 2011. Development and application of a physically based landscape water balance in the SWAT model. Hydrological Processes, 25(6): 915-925.

Woldesenbet, T.A., Elagib, N.A., Ribbe, L., Heinrich, J., 2017a. Gap filling and homogenization of climatological datasets in the headwater region of the Upper Blue Nile Basin, Ethiopia. International Journal of Climatology, 37(4): 2122-2140.

Woldesenbet, T.A., Elagib, N.A., Ribbe, L., Heinrich, J., 2017b. Hydrological responses to land use/cover changes in the source region of the Upper Blue Nile Basin, Ethiopia. Science of the Total Environment, 575: 724-741.

Yan, B., Fang, N., Zhang, P., Shi, Z., 2013. Impacts of land use change on watershed streamflow and sediment yield: an assessment using hydrologic modelling and partial least squares regression. Journal of Hydrology, 484: 26-37.

Yin, J., He, F., Xiong, Y.J., Qiu, G.Y., 2017a. Effects of land use/land cover and climate changes on surface runoff in a semi-humid and semi-arid transition zone in northwest China. Hydrology and Earth System Sciences, 21(1): 183-196.

Yin, J., He, F., Xiong, Y.J., Qiu, G.Y., 2017b. Effects of land use/land cover and climate changes on surface runoff in a semi-humid and semi-arid transition zone in northwest China. Hydrology and Earth System Sciences, 21(1): 183.

Yue, S., Pilon, P., Phinney, B., Cavadias, G., 2002. The influence of autocorrelation on the ability to detect trend in hydrological series. Hydrological Processes, 16(9): 1807-1829.

Yue, S., Wang, C., 2004. The Mann-Kendall test modified by effective sample size to detect trend in serially correlated hydrological series. Water Resources Management, 18(3): 201-218.

Table 1: The UBNRB's ~~Areal~~ areal long term (1971––2010) mean annual and seasonal rainfall and streamflow ~~of UBNRB~~

| Station | Amount | | | | Contribution (%) | | | | |
|---|---|---|---|---|---|---|---|---|---|
| | Kiremit | Belg | Bega | Total | Kiremit | Belg | Bega | Mean | Area (km$^2$) |
| Flow (m$^3$s$^{-1}$) | 3506.3 | 300.4 | 1018.4 | 4825.1 | 72.7 | 6.2 | 21.1 | 1608 | 172,254 |
| Flow (BCM) | 36.4 | 3.1 | 10.6 | 50.7 | | | | | |
| Rainfall (mm) | 1070.1 | 140.8 | 238.9 | 1449.8 | 73.8 | 9.7 | 16.5 | | |

Kiremit: long rainy season, Belg: ~~Short~~ short rainy season, Bega: ~~Dry~~ dry season

Table 2: Data sets ~~of~~ for the baseline and altered periods for the SWAT simulation used to analy~~z~~se the combined and isolated~~single~~ effect of LULC and climate changes on streamflow and water balance components

| Model run ~~n~~No. | Combined effect | | Isolated LULC change effect | | Isolated climate change effect | | Remark |
|---|---|---|---|---|---|---|---|
| | Climate data set | LULC map | Climate data set | LULC map | Climate data set | LULC map | |
| 1 | 1970s | 1973 | 1970s | 1973 | 1970s | 1973 | Base period |
| 2 | 1980s | 1985 | 1970s | 1985 | 1980s | 1973 | altered P~~p~~eriod1 |
| 3 | 1990s | 1995 | 1970s | 1995 | 1990s | 1973 | altered P~~p~~eriod2 |
| 4 | 2000s | 2010 | 1970s | 2010 | 2000s | 1973 | altered P~~p~~eriod3 |

Table 3: MK and Pettitt tests for the UBNRB's rainfall and streamflow of UBNRB after TFPW at different time scales

| | Stream flow | | | | | Rainfall | | | | |
| | p-value | | | | | p-value | | | | |
| Time scale | After* | Before* | Sen's slope: | Change point | Pettit test | After* | Before* | Sen's slope | Change point | Pettit test |
|---|---|---|---|---|---|---|---|---|---|---|
| Daily | < 0.0001 | < 0.0001 | 0.013 | 1987 | Increasing | 0.387 | 0.953 | 0.000 | 1988 | Increasing |
| Monthly | < 0.0001 | 0.031 | 0.378 | | No change | 0.010 | 0.640 | 0.009 | | No change |
| annually | < 0.0001 | 0.009 | 9.619 | 1995 | Increasing | 0.006 | 0.260 | 1.886 | | No change |
| Kiremit | < 0.0001 | 0.014 | 20.30 | | No change | 0.010 | 0.348 | 1.364 | | No change |
| Belg | < 0.0001 | 0.004 | 3.593 | 1985 | Increasing | 0.822 | 0.935 | 0.068 | | No change |
| Bega | 0.000 | 0.214 | 4.832 | | No change | 0.527 | 0.755 | 0.169 | | No change |

* Bbefore and after TFPW:, p: probability at 5% significance level

Table 4: Summary of the UBNRB's precipitation indices of the UBNRB at decadal time series

| Indices | 1970s | 1980s | 1990s | 2000s |
|---|---|---|---|---|
| Mean (mm) | 4.17 | 4.05 | 4.42 | 4.16 |
| 95 percentile (mm) | 12.57 | 12.52 | 13.66 | 13.31 |
| 99 percentile (mm) | 17.34 | 17.77 | 19.44 | 19.65 |
| 1-day max (mm) | 27.15 | 25.67 | 32.24 | 32.38 |
| R20mm (days) | 16 | 15 | 30 | 35 |
| SDII (mm/day) | 7.22 | 7.38 | 7.66 | 7.77 |

SDII is the ratio of total precipitation (mm) to R1mm (days).

Table 5: Confusion (error) matrix for the 2010 land use/cover classification map

| LULC class | Water | Forest | Cultivated | Bushes and sShrubs | Row total | Producers' accuracy |
|---|---|---|---|---|---|---|
| Water | 44 | 0 | 0 | 0 | 44 | 100 |
| Forest | 1 | 46 | 6 | 8 | 61 | 75.4 |
| Cultivated land | 2 | 3 | 77 | 15 | 97 | 79.4 |
| Bushes and shrubs | 1 | 3 | 9 | 73 | 86 | 84.9 |
| Column total | 48 | 52 | 92 | 86 | 288 | |
| User's accuracy (%) | 91.7 | 88.5 | 83.7 | 84.9 | | |
| Over all accuracy(%) | 0.880 | | | | | |
| Kappa | 0.77 | | | | | |

Table 6: The SWAT model's sStatistical performance measure values of the SWAT model

| Period | | $R^2$ | NSE | RVE (%) |
|---|---|---|---|---|
| 1970s | Calibration (1973–1977) | 0.79 | 0.74 | −3.41 |
| | Validation (1978–1980) | 0.84 | 0.83 | 7.18 |
| 1980s | Calibration (1983–1987) | 0.80 | 0.74 | −0.72 |
| | Validation (1988–1990)9 | 0.86 | 0.82 | 0.73 |
| 1990s | Calibration (1993–1997) | 0.91 | 0.91 | 1.79 |
| | Validation (1998–2000) | 0.87 | 0.84 | −3.56 |
| 2000s | Calibration (2003–2007) | 0.86 | 0.86 | 3.99 |
| | Validation (2008–2010) | 0.94 | 0.92 | −7.51 |

Table 7: SWAT sensitive model parameters and their (final) calibrated values for the four model runs.

| Parameter | Optimum value | | | |
|---|---|---|---|---|
| | 1970s | 1980s | 1990s | 2000s |
| R-CN2 | 0.88 | 0.91 | 0.92 | 0.9 |
| a-Alpha-BF | 0.028 | 0.028 | 0.028 | 0.028 |
| V-GW_REVAPMN | 0.7 | 0.45 | 0.7 | 0.34 |
| V-GWQMN | 750 | 750 | 750 | 750 |
| V-REVAPMN | 550 | 450 | 425 | 550 |
| a-ESCO | −0.85 | −0.85 | −0.85 | −0.85 |
| R-SOL_AWC | 6.5 | 6.5 | 6.5 | 6.5 |

R: value from the SWAT database is multiplied by a given value:, V: rReplace the initial parameter by the given value:, a: aAdding the given value to initial parameter value.

Table 8: Water–balance–components analysis in the Upper Blue Nile River Basin (mm/year) by considering LULC and climate change over respective periods. All streamflow estimates are for– El Diem station.

| Water balance components | 1970s | 1980s | 1990s | 2000s |
|---|---|---|---|---|
| Surface flow (Qs) | 112.8 | 143.4 | 168.6 | 141.4 |
| Lateral flow (Ql) | 116.8 | 113.35 | 125.9 | 117.6 |
| Base flow (Qb) | 47.3 | 29.6 | 9.8 | 64.7 |
| PET (mm) | 1615.1 | 1627.3 | 1614.7 | 1732.9 |
| Ea (mm) | 871.6 | 852.6 | 904.3 | 885 |
| Precipitation (P) | 1428.1 | 1397.1 | 1522.2 | 1462.5 |
| Total yield ( Qt) | 276.9 | 286.3 | 304.3 | 323.7 |
| Qs/Qt (%) | 40.7 | 50.1 | 55.4 | 43.7 |
| Qb/Qt (%) | 17.1 | 10.3 | 3.2 | 20.0 |
| Ea/P (%) | 61.0 | 61.0 | 59.4 | 60.5 |

| Qt/P (%) | 19.4 | 20.5 | 20.0 | 22.1 |
| --- | --- | --- | --- | --- |

Figure 1 : Locations of study area and meteorological and discharge stations, with the Digital Elevation Model (DEM) data as the background

**Figure 2**: Schematic representation of the SWAT model structure from (Marhaento *et al.*, 2017)
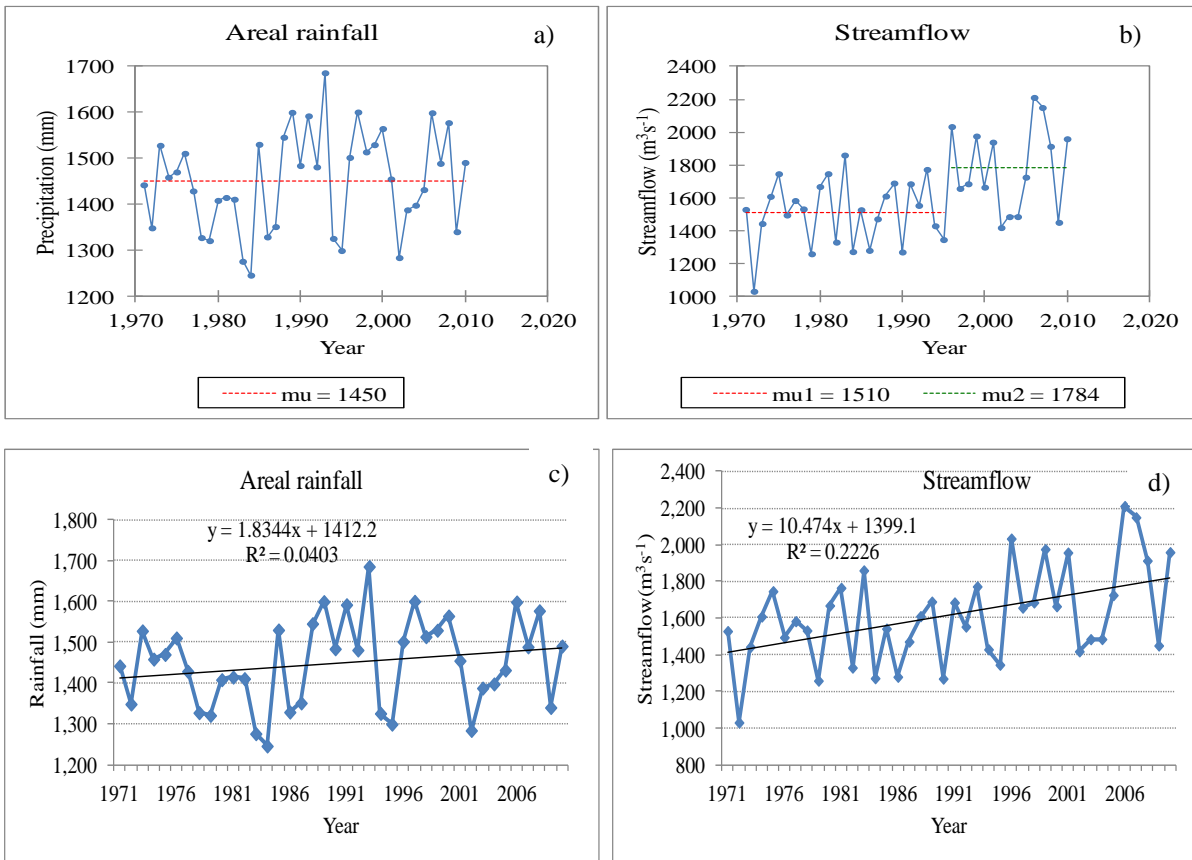
Figure 3: The Pettitt homogeneity test a) annual rainfall, b) annual flow of the UBNRB, cC) linear trend of mean annual rainfall and d) linear trend of mean annual streamflow.
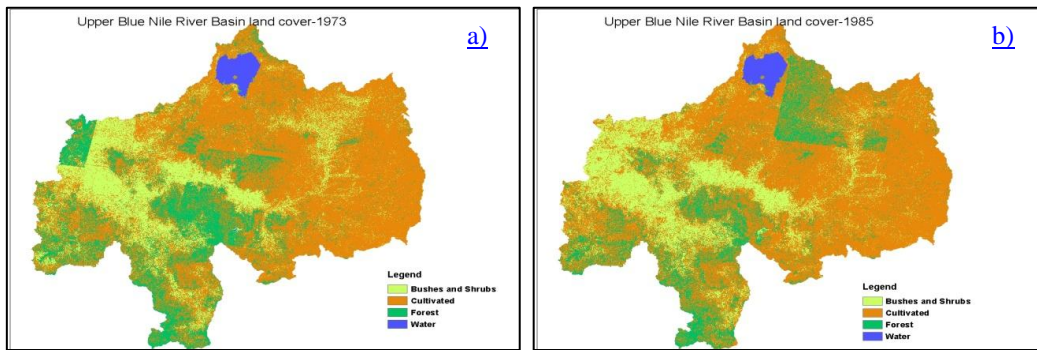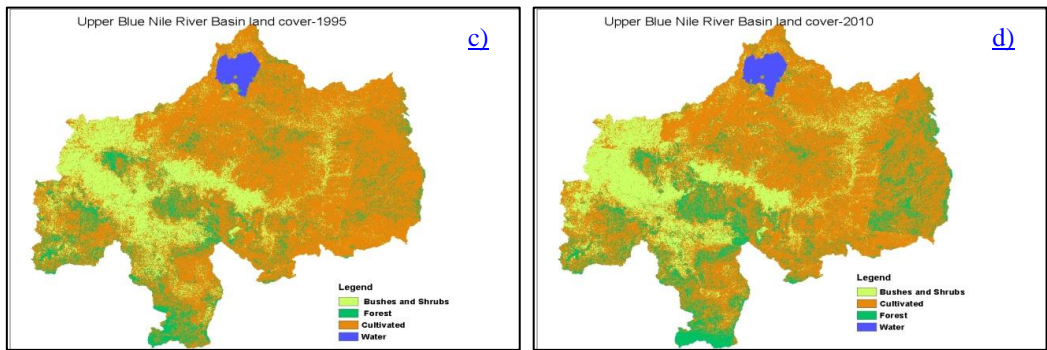
Figure 4: Landcover map of UBNRB derived from Landsat images– a) 1973, b) 1985, c) 1995, and d) 2010

a)

-b)
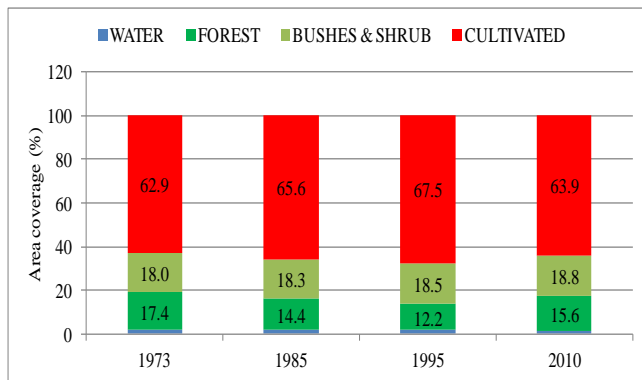
Figure 5: a) LULC composition, b) LULC change in the UBNRB during the period from 1973 to 2010

a)
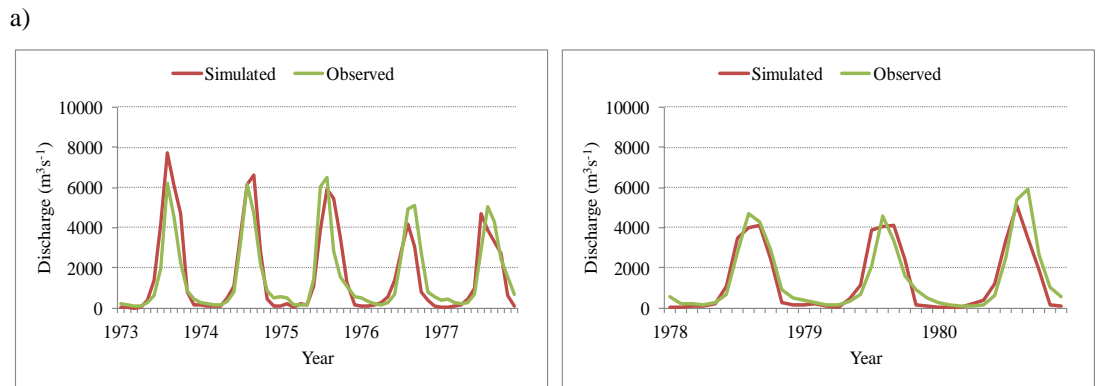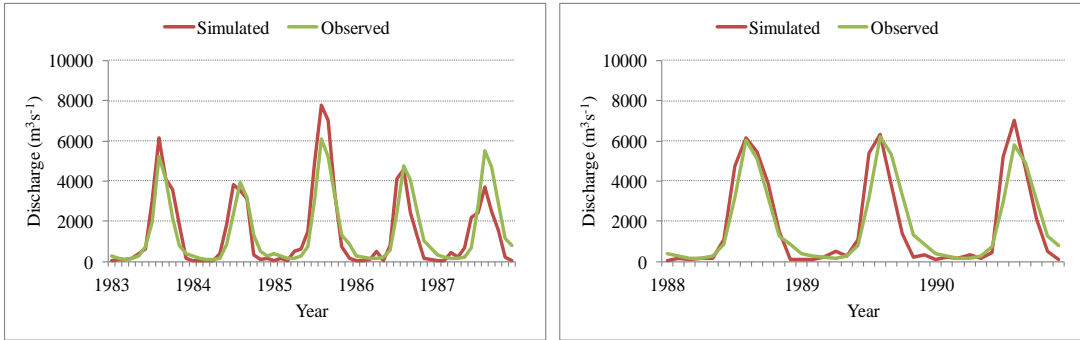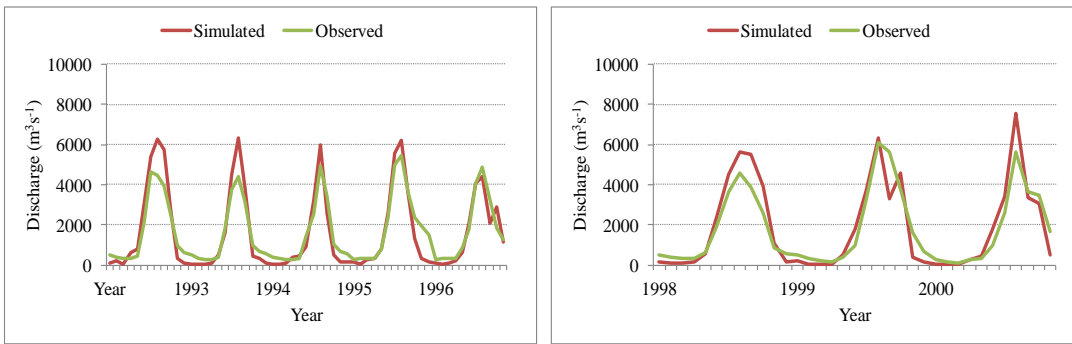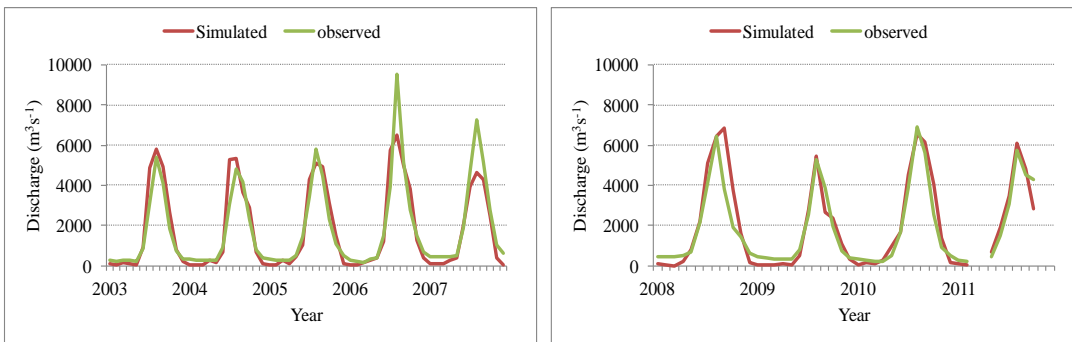
Figure 6: Calibration and validation of the SWAT hydrological model (left and right) respectively a) 1970s, b) 1980s, c) 1990s, and d) 2000s monthly time scale
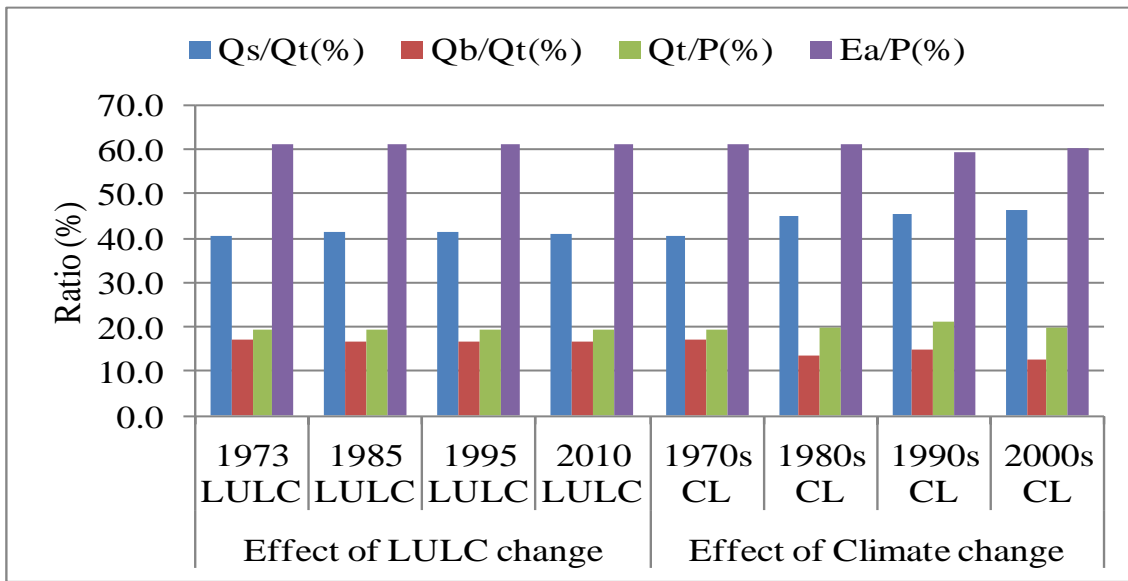
Figure 7: Ratio of water balance component analysis at the El Diem station using a singlean isolated effect (LULC/climate change).